

Reduced Barrier for Ion Migration in Mixed-Halide Perovskites

Lucie McGovern, Gianluca Grimaldi, Moritz H. Futscher, Eline M. Hutter, Loreta A. Muscarella, Moritz C. Schmidt, and Bruno Ehrler*

Cite This: <https://doi.org/10.1021/acsaem.1c03095>

Read Online

ACCESS |

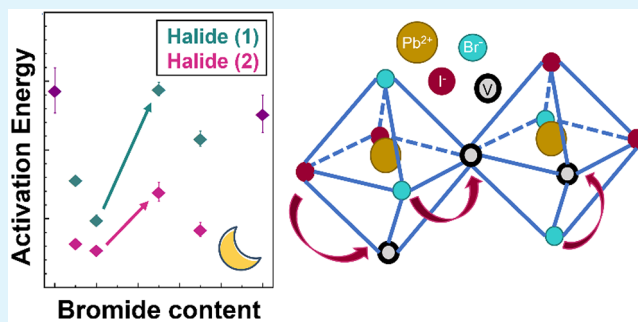
Metrics & More

Article Recommendations

Supporting Information

ABSTRACT: Halide alloying in metal halide perovskites is a useful tool for optoelectronic applications requiring a specific bandgap. However, mixed-halide perovskites show ion migration in the perovskite layer, leading to phase segregation and reducing the long-term stability of the devices. Here, we study the ion migration process in methylammonium-based mixed-halide perovskites with varying ratios of bromide to iodide. We find that the mixed-halide perovskites show two separate halide migration processes, in contrast to pure-phase perovskites, which show only a unique halide migration component. Compared to pure-halide perovskites, these processes have lower activation energies, facilitating ion migration in mixed versus pure-phase perovskites, and have a higher density of mobile ions. Under illumination, we find that the concentration of mobile halide ions is further increased and notice the emergence of a migration process involving methylammonium cations. Quantifying the ion migration processes in mixed-halide perovskites shines light on the key parameters allowing the design of bandgap-tunable perovskite solar cells with long-term stability.

KEYWORDS: perovskite, ion migration, phase segregation, mixed halide, transient ion drift, activation energy, halide, methylammonium



INTRODUCTION

Perovskite solar cell efficiencies have increased rapidly in the past decade and now reach an impressive 25.5% power conversion efficiency in single-junction cells, closely matching up with the 26.7% record for silicon solar cells.¹ On top of these high efficiencies, another key advantage with perovskites lies in the bandgap tunability of the material, easily achievable through mixing of the A, B, and X elements composing the ABX₃ perovskite structure.² For example, halide alloying has been shown to allow for a large variation in the bandgap, from 1.6 to 3.2 eV in methylammonium-based MAPbX_nY_{3-n} perovskites, with (X,Y) consisting of either I, Br, or Cl. The main factor impeding large-scale commercialization of perovskite devices remains the issue of their stability in time, with only a handful of perovskite devices showing the necessary stability under accelerated lifetime conditions. In that regard, the more intrinsically stable the perovskite layer, the easier it will be to stabilize the full device.

For mixed-halide systems, the instability is commonly observed through the photoinduced phase segregation process, in which light induces demixing of the perovskite composition, leading to the formation of iodide-rich and bromide-rich phases within the film.³ Photoinduced phase segregation relies on the migration of the halide species through the perovskite film, linking it to the larger topic of ion migration in perovskite solar cells. At its core, ion migration is a process by which ions from the lead halide APbX₃ structure become mobile and hop

through the perovskite lattice. This leads to long-term stability issues, as the process might not be fully reversible.⁴⁻⁶ Combining bandgap tunability with long-term stability is crucial for the further development of perovskite devices. To this end, a better understanding of the ion migration process in mixed-halide systems is needed, to determine specific parameters of influence that can aid in mitigating or suppressing this feature altogether.

During illumination, the observation of halide ion migration is easily accessible through monitoring of the photoinduced phase segregation, using UV/visible absorption, PL emission spectroscopy, and/or transient absorption spectroscopy.⁷⁻¹⁴ In the absence of segregation, however, which is the case when the cells are in the dark or when the mixing ratio of bromide to iodide falls below the 0.2 threshold,³ we need other tools to characterize the ion migration processes at play. So far there have only been a limited number of studies focusing on these regimes, using AC impedance spectroscopy or DC polarization measurements.^{15,16} Although these works shed light on ion

Received: October 15, 2021

Accepted: December 6, 2021

migration in mixed-halide perovskites, the full picture remains elusive, specifically whether the trends observed stem from iodide or bromide migration, and how to attribute the relative contributions to the ion migration process, in terms of migration activation energy, ion diffusion coefficient, and concentration of mobile ions.

Transient ion drift (TID) can be used for ion migration measurement in dark as well as light conditions and provides a detailed description of the process, revealing the nature of the mobile ion (whether anion or cation), and allowing for the quantification of the activation energy E_a , the diffusion coefficient D_{ion} , and the concentration N_{ion} of mobile ions.^{17,18} With this work, we aim to answer the following questions: (i) how does the mixing ratio of bromide to iodide change the ion migration process for the perovskite devices and (ii) how does light affect this ion migration process. To answer these questions, we prepare perovskite solar cells with varying ratios of bromide to iodide, measure the TID capacitance transients in these devices, and finally fit these transients to extract the ion migration characteristics E_a , D_{ion} , and N_{ion} of the various mixed-halide perovskite compositions.

RESULTS AND DISCUSSION

To study the effect of the bromide to iodide ratio on the ion migration process, we prepare solar cell devices with the composition $\text{MAPb}(\text{Br}_x\text{I}_{1-x})_3$ and vary the x ratios ($x = 0.1, 0.2, 0.5, \text{ and } 0.7$) following a synthesis described in Supporting Information S1. For reliable comparison with our previously published pure halide devices,^{19,20} we use the same device structure (see Figure 1a). To characterize these devices,

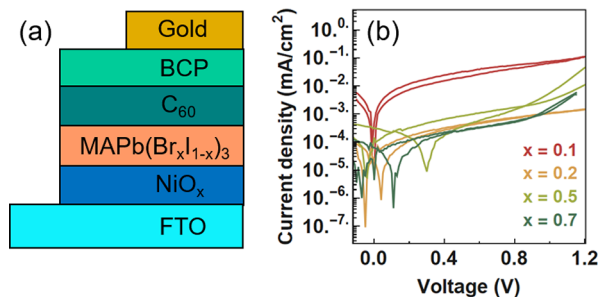


Figure 1. (a) P-i-n device architecture of the $\text{MAPb}(\text{Br}_x\text{I}_{1-x})_3$ perovskite solar cells, using $x = 0.1, 0.2, 0.5, \text{ and } 0.7$, and their corresponding (b) dark IV curves measured with a scan speed of 10 mV s^{-1} , presented on a semilog scale.

dark IV curves are presented in Figure 1b. These curves show a hysteretic behavior for most of the solar cells considered, an effect typically associated with the formation of interfacial charges between the perovskite and the transport materials.²¹ The main requirement for successful TID characterization is a low series resistance, so that the measured signal can be related to the capacitance of the perovskite when a small AC voltage is applied. The series resistance is determined by fitting the Nyquist plots (see Supporting Information S2) and is found to be below $20 \Omega \text{ cm}^2$ throughout the bromide to iodide ratios used in this study. The dark IV curves presented here are consistent with those found in the literature for devices with similar perovskite and transport materials.²²

TID is an electronic spectroscopy technique aimed at characterizing ion migration processes in semiconductor devices.^{17,18} We measure the capacitance transients of the

$\text{MAPb}(\text{Br}_x\text{I}_{1-x})_3$ perovskite solar cells at different temperatures after applying a voltage pulse of 1.5 V for 2 s . We note that we choose the 1.5 V voltage pulse such that it is both high enough to detect the ion dynamics with TID (see the comparison with TID after application of voltage biases of 1 or 1.25 V in Supporting Information S2) while remaining below the threshold for electrically induced phase segregation.^{23,24} The results are plotted in Figure 2 as the relative difference in capacitance, i.e., $\Delta C = C(t) - C_0$, with $C(t)$ the capacitance as a function of time and C_0 the capacitance at time $t = 0$. These transients already provide a qualitative picture of ion migration in these mixed-halide perovskite systems. In the dark, we find that the capacitance decays for all the halide ratios considered. In p-type perovskites, negative capacitance transients are associated with migration from an anion species. Because the only negatively charged species in ABX_3 is the X^- halide ion, this signals migration from a halide species. This assignment is similar to what we have previously found in both pure-halide perovskites, MAPbI_3 and MAPbBr_3 .^{19,20} Note that the doping of the perovskite layer is a matter of active debate (assigned to n-type,²⁵ p-type,²⁶ and intrinsic²⁷). The observed feature could thus correspond to halide migration, but other assignments remain possible (cation migration in an n-type material, cation vacancy migration in a p-type material). The negative feature observed here shares many properties with halide migration observed directly,^{28,29} and we hence assign it to halide migration for the remainder of the discussion. For $x = 0.1$, there is a small positive signal visible for the highest temperatures, at 315 and 330 K , but this positive trend remains very small compared to the main negative trend observed.

We additionally measure the capacitance transients under illumination for $x = 0.1$ and 0.2 . The devices with $x = 0.5$ and 0.7 could not be measured during illumination, because the light-induced phase segregation would change the sample in a nonreversible way during the capacitance measurements. The results under illumination show a different picture than those in the dark, where on top of the negative transient present at all temperatures, a new positive trend becomes clearly visible after 100 to 200 ms , for the whole temperature range considered. Because we are considering p-type perovskites, we attribute this positive trend to cation migration. As lead migration is energetically unfavorable,³⁰ we assign the feature to methylammonium cation migration. Finally, we also observe a general growth in the magnitude of the negative capacitance transients compared to dark conditions. Under light conditions, the relative capacitance difference is highest for $x = 0.2$, with $\Delta C = -10 \text{ nF cm}^{-2}$.

To obtain a more quantitative picture of the ion migration process, we fit the TID capacitance transients to the following equation:

$$C(t, T) = C_\infty(T) + \sum_n \Delta C_n(T) \exp\left(\frac{-t}{p_{\text{fit}(n)} T \exp\left(\frac{E_a(n)}{k_B T}\right)}\right) \quad (1)$$

where $C(t, T)$ is the capacitance as a function of time and temperature, $C_\infty(T)$ is the steady-state value of the capacitance at a certain temperature T , $\Delta C_n(T)$ is the capacitance magnitude at temperature T of the process n , $p_{\text{fit}(n)}$ is a fitted parameter for process n that depends on the diffusion coefficient, and E_a is the activation energy of the process n .

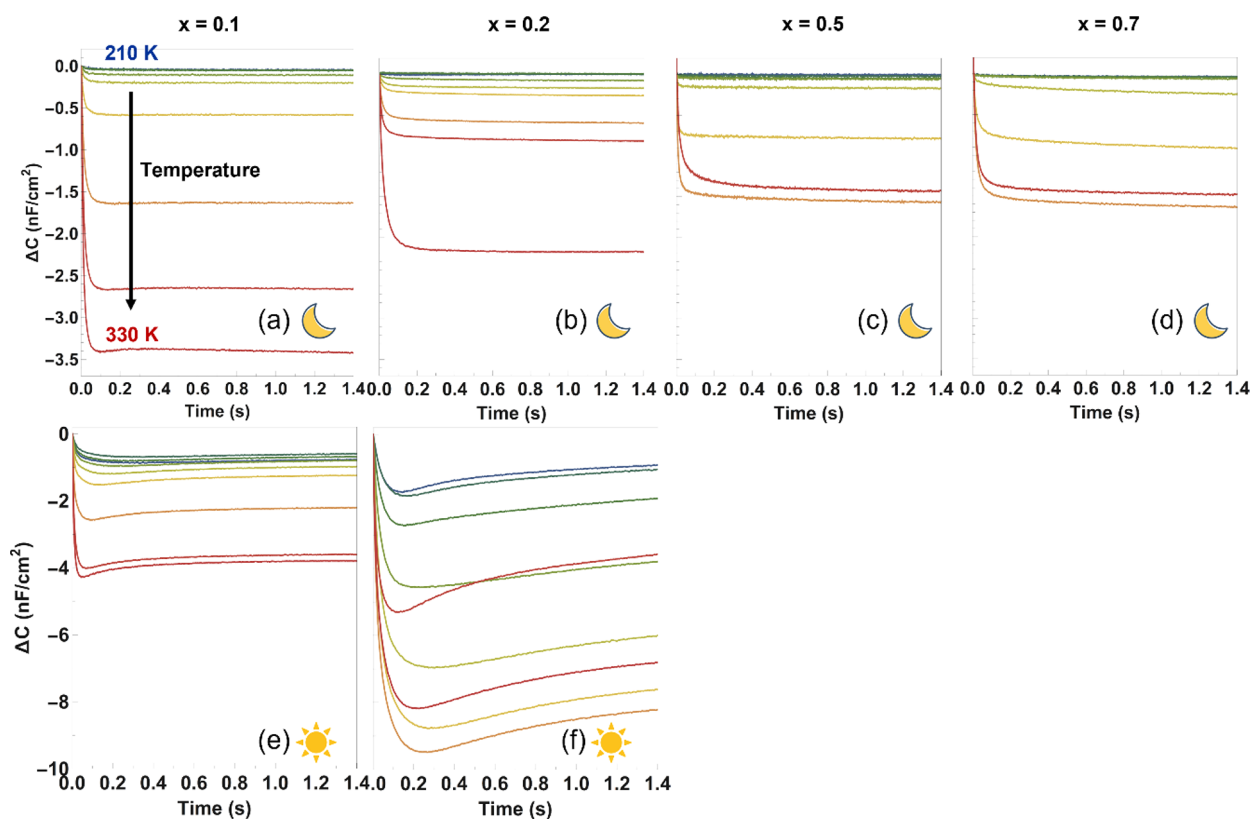


Figure 2. Relative difference in capacitance transients $\Delta C = C(t) - C_0$ of the $\text{MAPb}(\text{Br}_x\text{I}_{1-x})_3$ solar cells, measured with an AC voltage of 20 mV, after applying a voltage pulse of 1.5 V for 2 s, under dark conditions for $x =$ (a) 0.1, (b) 0.2, (c) 0.5, and (d) 0.7, and during illumination for $x =$ (e) 0.1 and (f) 0.2. The transients shown here are taken at temperatures of 210, 225, 240, 255, 270, 285, 300, 315, and 330 K. Light conditions correspond to a 405 nm CW laser shining directly on the considered pixel, with a power density of 1.59 W cm^{-2} .

Every migration pathway would correspond to an individual exponential decay, and for the mixed-halide perovskites, we can fit the data with two or three decay traces, respectively, under dark and illumination conditions.

The fit is obtained by using a global fit algorithm as described in Supporting Information S3. The values obtained for the ion migration activation energy, the ion diffusion coefficient, and the density of mobile ions are shown in Figure 3. For comparison, we add the values for MAPbI_3 and MAPbBr_3 , reproduced from refs 19 and 20. When fitting the capacitive transients, we find that we need two exponential contributions to correctly fit the negative peak, whether in dark or in light, and across the full composition range from $x = 0.1$ to $x = 0.7$. This means that for methylammonium-based mixed-halide perovskites, there are two halide migration processes at play, either from the iodide and the bromide species, or from the combination of a grain boundary process with a bulk process, similar to what we have previously observed for MAPbBr_3 cells with varying grain size.³¹ This is in stark contrast with the single halide migration process happening in the pure-phase halide perovskites. The small positive peak present in dark for $x = 0.1$ is too low to be fitted, suggesting that the concentration of mobile methylammonium ions in this case is below $1 \times 10^{14} \text{ cm}^{-3}$ (considering the hypothesis of a high doping density of 10^{17} cm^{-3} , see Supporting Information S2 and S3). To fit the capacitance transients taken under illumination, we used three exponential contributions, where two are assigned to the negative halide peaks and one to the positive methylammonium peak.

Looking at Figure 3a, we notice that both activation energies from the halide migration process are decreased in mixed-halide compositions compared to the single-ion migration activation energies from the pure-halide compositions. Specifically, for the first process contributing to halide migration, with highest activation energy, labeled Halide (1) in Figure 3, the activation energy is most decreased in the low-bromide regime, with $E_a = 157 \pm 3 \text{ meV}$ for $x = 0.1$ and $E_a = 98 \pm 7 \text{ meV}$ for $x = 0.2$, then increases to $E_a = 289 \pm 10 \text{ meV}$ for $x = 0.5$ and $E_a = 217 \pm 11 \text{ meV}$ for $x = 0.7$. The trend is similar for the second process contributing to halide migration, with lower activation energy, labeled Halide (2) in Figure 3, with a maximal value of $E_a = 139 \pm 14 \text{ meV}$ for $x = 0.5$. García-Rodríguez et al.¹⁵ showed an increase in the activation energy with higher bromide concentration, in their case using bromide concentrations below 10%. Here, we find that halide migration has a lower activation energy in mixed devices for bromide contents of 10, 20, 50, and 70%.

Figure 3b shows the halide diffusion coefficients in the dark. The diffusion coefficient of both contributions is constant for different bromide concentrations. The diffusion coefficient of Halide (1) is on the order of 1×10^{-9} to $1 \times 10^{-10} \text{ cm}^2 \text{ s}^{-1}$, similar—within the error bar—to the iodide and bromide diffusion coefficients in MAPbI_3 and MAPbBr_3 . Halide (2) on the other hand is slower, on the order of $1 \times 10^{-11} \text{ cm}^2 \text{ s}^{-1}$. Halide migration is thus equally fast in the mixed devices.

Figure 3c shows the density of mobile halide ions. The Halide (2) peak has a relatively constant and similar concentration to the bromide and iodide mobile ion densities found in the pure-phase perovskites. The peak for Halide (1)

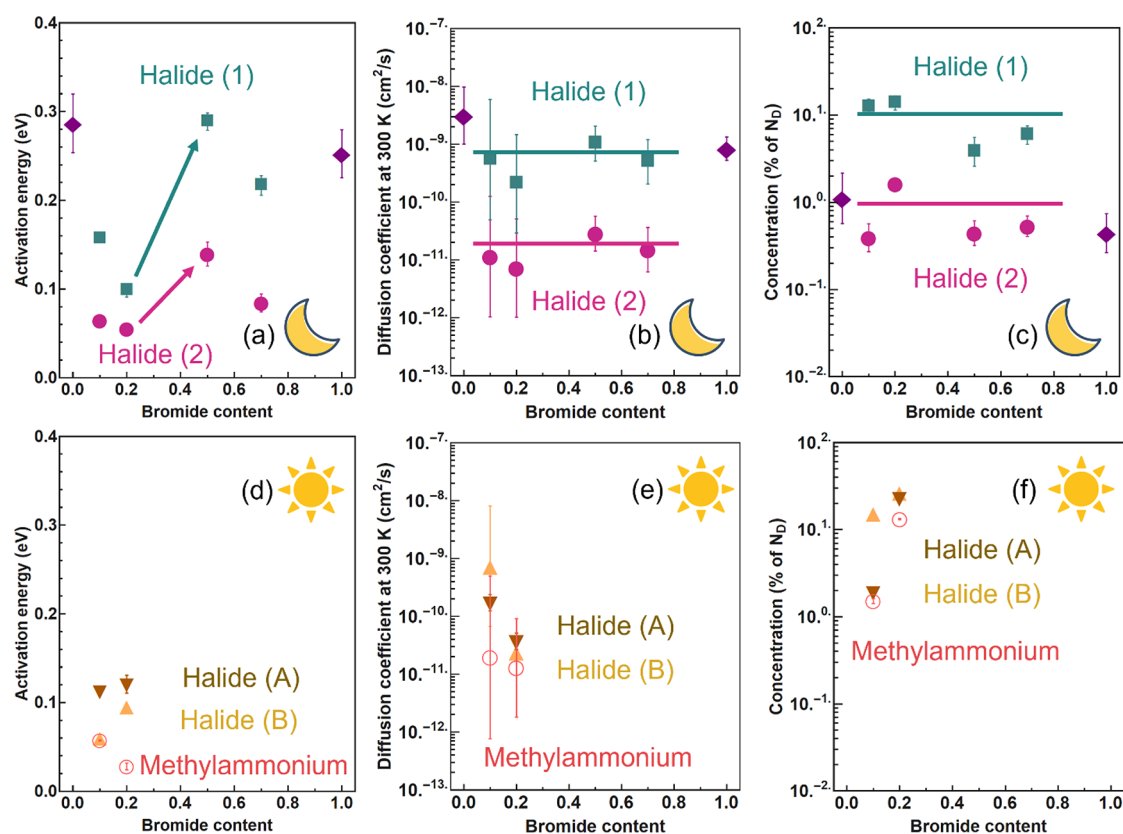


Figure 3. Comparison of the characteristics of ion migration as a function of the bromide to iodide ratio. Halide ion migration characteristics in dark, with (a) ion migration activation energies, (b) halide ion diffusion coefficients at 300 K, and (c) concentration of mobile halide ions, represented as a fraction of the doping density. The two migration processes Halide (1) and Halide (2) are shown in blue and pink, respectively. The arrows in panel a represent the point of phase transition, the lines in panels b and c are a guide to the eye representing the weighted averages for diffusion coefficient and mobile ion concentration. The ion migration characteristics in light are respectively shown in dark and light orange for Halide (A) and Halide (B) and in red for methylammonium, with (d) ion migration activation energies, (e) halide and methylammonium ion diffusion coefficients at 300 K, and (f) concentration of mobile ions. Error bars represent the standard deviation of the fit parameters giving lowest chi-square values (see S3). The values for $x = 0$ and 1 are reproduced from refs 19 and 20.

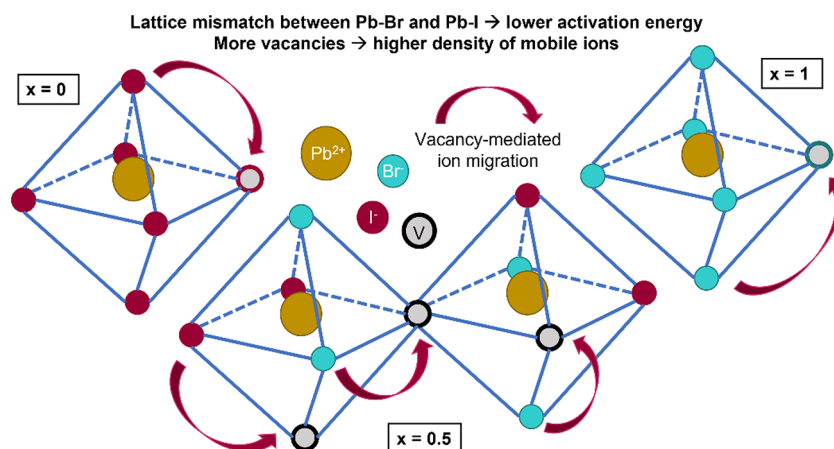


Figure 4. Schematic picture of the ion migration process in the pure-halide perovskites compared to the mixed-halide perovskites. The lattice mismatch between the bromide and iodide perovskite lattices in the mixed-halide case leads to a decreased activation energy for the migration step. The number of vacancies is also higher for the mixed-halide case, thereby increasing the density of mobile halide ions in the mixed-halide perovskites.

on the other hand shows a clear increase in the concentration of migrating halide ions compared to the pure-phase cases, with up to 10% of the doping density for the devices with 10 and 20% bromide concentrations. There is thus more halide migration in the mixed devices.

One possible scheme to rationalize these observations is to consider the two processes separately. Halide (1) shows a high density of ions, which presumably arises from an increased density of vacancies when moving from pure-halide to mixed-halide compositions. The difference in solubility of iodide and

bromide species has indeed been suggested to result in heterogeneous nucleation during thin-film deposition³² and has led to the observation of lower crystallinity in the mixed films,³³ which could in turn lead to an increase in the density of halide vacancies. The Halide (1) process would thus become more prominent for mixed halides because of the higher number of vacancies. This is in line with the finding that the fraction of halide vacancies enables and controls the rate of phase segregation.^{9,34} Overall, the Halide (1) process shares many features with the halide migration in pure-halide perovskites. It has a similar diffusion coefficient and a slightly reduced activation energy, especially for the mixing ratios $x < 0.2$. This reduction in activation energy could be associated with the strain in the crystal from the different bond lengths between bromide and iodide,³⁵ in which case the activation energy should be lowest close to the phase transition. A reduced activation energy might naively lead to an increase diffusion coefficient. However, in the mixed halide perovskites, the entropy is likely to decrease when the ion is moving, as it is most likely coming from a well-mixed unit cell. The effect would be accentuated if the ions are moving toward a transport layer, as the mobile halide will accumulate there and likely end up in a unit cell enriched in one of the halides. The maximal entropy difference for a mobile halide ion to migrate is the entropy difference $\Delta S = k \ln\left(\frac{8!}{4! \times 4!}\right) = 3.6 \times 10^{-4} \text{ eV K}^{-1}$, where the argument of the logarithm represents the ratio between the number of possible configurations for the neighbors of an ion in a mixed-halide phase ($8!/(4! \times 4!)$) and the number of configurations for neighboring ions in a single-halide phase (1). Although we expect this effect to be large in the well-mixed perovskites ($x < 0.2$), the higher bromide ratios already show some demixing even in the dark and when a bias is applied,^{36,37} which means that the entropy change during migration toward the interfaces is smaller. Taken together, the reduced activation energy and entropy gain appear to balance each other, resulting in a rather constant diffusion coefficient at room temperature. A representation of this scheme is depicted in Figure 4.

Halide (2) represents a very slow ion with a low activation energy. The diffusion coefficient is about 2 orders of magnitude lower than that of Halide (1). Presumably, even if present, this process cannot be detected easily in pure-halide mixtures as the concentration is also about 2 orders of magnitude lower than Halide (1). We speculate that a similar process could be responsible for the very slow dynamics (minutes to days) often seen in perovskite devices.³⁸ The observation of the difference in the activation energy for migration before and after the $x = 0.2$ mark, with much lower migration barriers for the perovskites with low-bromide content, is also noteworthy. The $x \geq 0.2$ threshold marks the onset of light-induced phase segregation in mixed-halide perovskites and is thought to arise because of the phase transition (from tetragonal to cubic) close to this composition. Here this threshold is clearly visible in the ion migration properties of the devices, reinforcing the relationship between perovskite composition, phase segregation, and ion migration instability.

When comparing halide migration in dark and in light, we find that the activation energy is decreased in light; for instance, for the perovskite with 10% bromide, there is a small decrease from $65 \pm 5 \text{ meV}$ to $60 \pm 3 \text{ meV}$ for the first peak and a larger decrease from $157 \pm 3 \text{ meV}$ to $113 \pm 4 \text{ meV}$ for

the second peak. This is consistent with our previous work on these systems.¹⁴ We note that the similar activation energies between Halide (1) and Halide (A) seem to suggest the same process, but that TID cannot distinguish mechanisms, complicating the assignments of the Halide (1) and Halide (2) peaks in light. We thus choose the nomenclature Halide (A) and Halide (B) for the halide migration peaks in light. When comparing the diffusion coefficients in dark and in light, no clear trend seems to emerge, as there is both an increase in one of the features and a decrease in the other. The most noticeable difference lies in the concentration of mobile halide ions, with a clear increase in the total halide concentration as a function of doping density, from 12.8 to 17.3% for $x = 0.1$, and from 15.4 to 36.9% for $x = 0.2$. Under light, there is thus an increased halide ion migration, partly due to a lower activation energy and mostly due to the much larger fraction of mobile halide ions. We note that at such high densities, the quantification of ion migration by TID might not be accurate anymore because the analysis method assumes that the change in the charge density from mobile ions is small compared to the background doping density.

As mentioned above, in the presence of light, a new cation migration process appears for devices with $x = 0.1$ and 0.2 , on top of the halide migration process. This process has a very low activation energy ($<0.060 \text{ eV}$), has a low diffusion coefficient on the order of $1 \times 10^{-11} \text{ cm}^2 \text{ s}^{-1}$, and is prominent, representing 1.5 and 13.2% of the doping density, respectively, for the devices with 10 and 20% bromide concentrations. So far, in the dark, we have observed MA^+ migration only in the case of the pure MAPbI_3 perovskite, and in this work as a minor contribution to the $\text{MAPbI}_{2.7}\text{Br}_{0.3}$ perovskite. In other words, the higher the bromide concentration, the more methylammonium migration is suppressed, as the bond between lead and halide gets stronger. Under light conditions, it thus seems like the barrier preventing cation migration is released, in agreement with galvanostatic measurements from Zhao et al.³⁹ showing decreased activation energies with increasing light intensity. This effect might happen either through an increase in the number of MA^+ vacancies in light—similar to the increase of halide vacancies observed in light⁴⁰—and/or through a loosening of the $\text{Pb}-\text{X}$ bond, perhaps upon polaron formation.^{41,42} We also note that one of the theories behind light-induced phase segregation involves polaron stabilization of the iodide domains. One possibility is that halide migration might promote this effect, whereas cation migration might prevent it; there, the reduction (or suppression) of cation migration in light when $x > 0.2$ would help rationalize the $x = 0.2$ threshold observed in light-induced phase segregation. This calls for future investigation.

All in all, light thus has a double effect on the ion migration process for the mixed-halide perovskites: first, it increases the number of mobile halide ions; second, it introduces an extra cation migration pathway. These results are in line with the previous work from Kim et al.,¹⁶ showing increased ionic conductivity in light compared to dark for similar perovskite compositions. In conductivity measurements, however, the contributions from diffusion coefficient and mobile ion density cannot be disentangled: here, we can thus specifically attribute the increased ion migration in light to an increase in the mobile ion density.

CONCLUSION

In conclusion, we find that mixing iodide and bromide in $\text{MAPb}(\text{Br}_x\text{I}_{1-x})_3$ solar cells facilitates halide ion migration by decreasing the activation energy and increasing the number of mobile halide ions. We also notice the appearance of a second pathway in the halide ion migration process, not observed in the pure-phase perovskites. In light, the density of mobile halide ions increases even more, and additional migration from the methylammonium cation becomes prominent. To reduce ion migration in mixed-halide perovskites, it is thus essential to increase the activation energy of the process and/or to decrease the density of mobile halide ions. These can be achieved, for instance, by applying pressure to the unit cell in the form of Cs^+ addition¹⁴ (E_a increase), or by tailoring the Pb:X stoichiometry to reduce the number of halide vacancies²⁶ (N_{ion} decrease). Our quantitative assessment of the ion migration processes in mixed-halide perovskites thus provides new insights into the relative contributions of activation energy, ion diffusion, and mobile ion density, tracing a path toward the rational design of mitigation strategies, which is necessary for the long-term stability of bandgap-tunable perovskite solar cells.

ASSOCIATED CONTENT

Supporting Information

The Supporting Information is available free of charge at <https://pubs.acs.org/doi/10.1021/acsaem.1c03095>.

Solar cell device fabrication; electrical measurements; fitting procedure (PDF)

AUTHOR INFORMATION

Corresponding Author

Bruno Ehrler – Center for Nanophotonics, AMOLF, Amsterdam 1098 XG, The Netherlands; orcid.org/0000-0002-5307-3241; Email: b.ehrler@amof.nl

Authors

Lucie McGovern – Center for Nanophotonics, AMOLF, Amsterdam 1098 XG, The Netherlands; orcid.org/0000-0001-7263-5249

Gianluca Grimaldi – Center for Nanophotonics, AMOLF, Amsterdam 1098 XG, The Netherlands; Cavendish Laboratory, University of Cambridge, Cambridge CB3 0HE, United-Kingdom; orcid.org/0000-0002-2626-9118

Moritz H. Futscher – Center for Nanophotonics, AMOLF, Amsterdam 1098 XG, The Netherlands; Laboratory for Thin Films and Photovoltaics, EMPA – Swiss Federal Laboratories for Materials Science and Technology, Dübendorf 8600, Switzerland; orcid.org/0000-0001-8451-5009

Eline M. Hutter – Center for Nanophotonics, AMOLF, Amsterdam 1098 XG, The Netherlands; Debye Institute for Nanomaterials Science, Utrecht University, Utrecht 3584 CB, The Netherlands; orcid.org/0000-0002-5537-6545

Loreta A. Muscarella – Center for Nanophotonics, AMOLF, Amsterdam 1098 XG, The Netherlands; orcid.org/0000-0002-0559-4085

Moritz C. Schmidt – Center for Nanophotonics, AMOLF, Amsterdam 1098 XG, The Netherlands

Complete contact information is available at: <https://pubs.acs.org/doi/10.1021/acsaem.1c03095>

Notes

The authors declare no competing financial interest.

ACKNOWLEDGMENTS

This work is part of the Dutch Research Council (NWO) and was performed at the research institute AMOLF. The work of L.M. and L.A.M. was supported by NWO Vidi Grant 016.Vidi.179.005. The work of G.G. was supported by the EPSRC International Centre to Centre grant EP/S030638/1. The work of M.H.F. was supported by NWO Project 15PR3202. The work of E.M.H. was supported by NWO. The work of M.C.S. was supported by the European Research Council (ERC), Grant agreement 947221. The authors thank Dr Sven Askes and Dr Christian Dieleman for carefully reading and commenting on the manuscript.

REFERENCES

- (1) Best Research-Cell Efficiency Chart | Photovoltaic Research | NREL. <https://www.nrel.gov/pv/cell-efficiency.html> (accessed 2021-10-09).
- (2) Sutherland, B. R.; Sargent, E. H. Perovskite Photonic Sources. *Nature Photonics* **2016**, *10*, 295–302.
- (3) Hoke, E. T.; Slotcavage, D. J.; Dohner, E. R.; Bowring, A. R.; Karunadasa, H. I.; McGehee, M. D. Reversible Photo-Induced Trap Formation in Mixed-Halide Hybrid Perovskites for Photovoltaics. *Chem. Sci.* **2015**, *6* (1), 613–617.
- (4) Cappel, U. B.; Svanström, S.; Lanzilotto, V.; Johansson, F. O. L.; Aitola, K.; Philippe, B.; Giangrisostomi, E.; Ovsyannikov, R.; Leitner, T.; Föhlich, A.; Svensson, S.; Mårtensson, N.; Boschloo, G.; Lindblad, A.; Rensmo, H. Partially Reversible Photoinduced Chemical Changes in a Mixed-Ion Perovskite Material for Solar Cells. *ACS Appl. Mater. Interfaces* **2017**, *9* (40), 34970–34978.
- (5) Gomez, A.; Sanchez, S.; Campoy-Quiles, M.; Abate, A. Topological Distribution of Reversible and Non-Reversible Degradation in Perovskite Solar Cells. *Nano Energy* **2018**, *45*, 94–100.
- (6) Domanski, K.; Roose, B.; Matsui, T.; Saliba, M.; Turren-Cruz, S. H.; Correa-Baena, J. P.; Carmona, C. R.; Richardson, G.; Foster, J. M.; De Angelis, F.; Ball, J. M.; Petrozza, A.; Mine, N.; Nazeeruddin, M. K.; Tress, W.; Grätzel, M.; Steiner, U.; Hagfeldt, A.; Abate, A. Migration of Cations Induces Reversible Performance Losses over Day/Night Cycling in Perovskite Solar Cells. *Energy Environ. Sci.* **2017**, *10* (2), 604–613.
- (7) Yoon, S. J.; Kuno, M.; Kamat, P. V. Shift Happens: How Halide Ion Defects Influence Photoinduced Segregation in Mixed Halide Perovskites. *ACS Energy Lett.* **2017**, *2* (7), 1507–1514.
- (8) Draguta, S.; Sharia, O.; Yoon, S. J.; Brennan, M. C.; Morozov, Y. V.; Manser, J. M.; Kamat, P. V.; Schneider, W. F.; Kuno, M. Rationalizing the Light-Induced Phase Separation of Mixed Halide Organic-Inorganic Perovskites. *Nat. Commun.* **2017**, *8* (1), 1–8.
- (9) Barker, A. J.; Sadhanala, A.; Deschler, F.; Gandini, M.; Senanayak, S. P.; Pearce, P. M.; Mosconi, E.; Pearson, A. J.; Wu, Y.; Srimath Kandada, A. R.; et al. Defect-Assisted Photoinduced Halide Segregation in Mixed-Halide Perovskite Thin Films. *ACS Energy Lett.* **2017**, *2* (6), 1416–1424.
- (10) Belisle, R. A.; Bush, K. A.; Bertoluzzi, L.; Gold-Parker, A.; Toney, M. F.; McGehee, M. D. Impact of Surfaces on Photoinduced Halide Segregation in Mixed-Halide Perovskites. *ACS Energy Lett.* **2018**, *3* (11), 2694–2700.
- (11) Elmelund, T.; Seger, B.; Kuno, M.; Kamat, P. V. How Interplay between Photo and Thermal Activation Dictates Halide Ion Segregation in Mixed Halide Perovskites. *ACS Energy Lett.* **2019**, *5* (1), 56–63.
- (12) Scheidt, R. A.; Kamat, P. V. Temperature-Driven Anion Migration in Gradient Halide Perovskites. *J. Chem. Phys.* **2019**, *151* (13), 134703.
- (13) Hutter, E. M.; Muscarella, L. A.; Wittmann, F.; Versluis, J.; McGovern, L.; Bakker, H. J.; Woo, Y.-W.; Jung, Y.-K.; Walsh, A.;

- Ehrler, B. Thermodynamic Stabilization of Mixed-Halide Perovskites against Phase Segregation. *Cell Reports Phys. Sci.* **2020**, *1* (8), 100120.
- (14) Muscarella, L. A.; Hutter, E. M.; Wittmann, F.; Woo, Y. W.; Jung, Y.-K.; McGovern, L.; Versluis, J.; Walsh, A.; Bakker, H. J.; Ehrler, B. Lattice Compression Increases the Activation Barrier for Phase Segregation in Mixed-Halide Perovskites. *ACS Energy Lett.* **2020**, *5* (10), 3152.
- (15) García-Rodríguez, R.; Ferdani, D.; Pering, S.; Baker, P. J.; Cameron, P. J. Influence of Bromide Content on Iodide Migration in Inverted MAPb(1-x)XBr₃ Perovskite Solar Cells. *J. Mater. Chem. A* **2019**, *7* (39), 22604–22614.
- (16) Kim, G. Y.; Senocrate, A.; Wang, Y. R.; Moia, D.; Maier, J. Photo-Effect on Ion Transport in Mixed Cation and Halide Perovskites and Implications for Photo-Demixing**. *Angew. Chem., Int. Ed.* **2021**, *60* (2), 820–826.
- (17) Heiser, T.; Weber, E. Transient Ion-Drift-Induced Capacitance Signals in Semiconductors. *Phys. Rev. B: Condens. Matter Mater. Phys.* **1998**, *58* (7), 3893–3903.
- (18) Futscher, M. H.; Gangishetty, M. K.; Congreve, D. N.; Ehrler, B. Quantifying Mobile Ions and Electronic Defects in Perovskite-Based Devices with Temperature-Dependent Capacitance Measurements: Frequency vs Time Domain. *J. Chem. Phys.* **2020**, *152* (4), 044202.
- (19) Futscher, M. H.; Lee, J. M.; McGovern, L.; Muscarella, L. A.; Wang, T.; Haider, M. I.; Fakharuddin, A.; Schmidt-Mende, L.; Ehrler, B. Quantification of Ion Migration in CH₃NH₃PbI₃ Perovskite Solar Cells by Transient Capacitance Measurements. *Mater. Horiz.* **2019**, *6* (7), 1497–1503.
- (20) McGovern, L.; Futscher, M. H.; Muscarella, L. A.; Ehrler, B. Understanding the Stability of MAPbBr₃ versus MAPbI₃: Suppression of Methylammonium Migration and Reduction of Halide Migration. *J. Phys. Chem. Lett.* **2020**, *11* (17), 7127–7132.
- (21) Weber, S. A. L.; Hermes, I. M.; Turren-Cruz, S. H.; Gort, C.; Bergmann, V. W.; Gilson, L.; Hagfeldt, A.; Graetzel, M.; Tress, W.; Berger, R. How the Formation of Interfacial Charge Causes Hysteresis in Perovskite Solar Cells. *Energy Environ. Sci.* **2018**, *11* (9), 2404–2413.
- (22) Lai, W. C.; Lin, K. W.; Guo, T. F.; Chen, P.; Liao, Y. Y. Perovskite-Based Solar Cells with Inorganic Inverted Hybrid Planar Heterojunction Structure. *AIP Adv.* **2018**, *8* (1), 015109.
- (23) Leijtens, T.; Hoke, E. T.; Grancini, G.; Slotcavage, D. J.; Eperon, G. E.; Ball, J. M.; De Bastiani, M.; Bowring, A. R.; Martino, N.; Wojciechowski, K.; McGehee, M. D.; Snaith, H. J.; Petrozza, A. Mapping Electric Field-Induced Switchable Poling and Structural Degradation in Hybrid Lead Halide Perovskite Thin Films. *Adv. Energy Mater.* **2015**, *5* (20), 1500962.
- (24) Vashishtha, P.; Halpert, J. E. Field-Driven Ion Migration and Color Instability in Red-Emitting Mixed Halide Perovskite Nanocrystal Light-Emitting Diodes. *Chem. Mater.* **2017**, *29* (14), 5965–5973.
- (25) Wang, Q.; Shao, Y.; Xie, H.; Lyu, L.; Liu, X.; Gao, Y.; Huang, J. Qualifying Composition Dependent p and n Self-Doping in CH₃NH₃PbI₃. *Appl. Phys. Lett.* **2014**, *105* (16), 163508.
- (26) Shi, T.; Yin, W. J.; Hong, F.; Zhu, K.; Yan, Y. Unipolar Self-Doping Behavior in Perovskite CH₃NH₃PbBr₃. *Appl. Phys. Lett.* **2015**, *106* (10), 103902.
- (27) Miyano, K.; Tripathi, N.; Yanagida, M.; Shirai, Y. Lead Halide Perovskite Photovoltaic as a Model p–i–n Diode. *Acc. Chem. Res.* **2016**, *49* (2), 303–310.
- (28) Xing, J.; Wang, Q.; Dong, Q.; Yuan, Y.; Fang, Y.; Huang, J. Ultrafast Ion Migration in Hybrid Perovskite Polycrystalline Thin Films under Light and Suppression in Single Crystals. *Phys. Chem. Chem. Phys.* **2016**, *18* (44), 30484–30490.
- (29) Luo, Y.; Khoram, P.; Brittman, S.; Zhu, Z.; Lai, B.; Ong, S. P.; Garnett, E. C.; Fenning, D. P. Direct Observation of Halide Migration and Its Effect on the Photoluminescence of Methylammonium Lead Bromide Perovskite Single Crystals. *Adv. Mater.* **2017**, *29* (43), 1703451.
- (30) Eames, C.; Frost, J. M.; Barnes, P. R. F.; O'Regan, B. C.; Walsh, A.; Islam, M. S. Ionic Transport in Hybrid Lead Iodide Perovskite Solar Cells. *Nat. Commun.* **2015**, *6* (1), 1–8.
- (31) McGovern, L.; Koschany, I.; Grimaldi, G.; Muscarella, L. A.; Ehrler, B. Grain Size Influences Activation Energy and Migration Pathways in MAPbBr₃ Perovskite Solar Cells. *J. Phys. Chem. Lett.* **2021**, *12* (9), 2423–2428.
- (32) Zhou, Y.; Poli, I.; Meggiolaro, D.; De Angelis, F.; Petrozza, A. Defect Activity in Metal Halide Perovskites with Wide and Narrow Bandgap. *Nat. Rev. Mater.* **2021**, *6*, 986–1002.
- (33) Rehman, W.; Milot, R. L.; Eperon, G. E.; Wehrenfennig, C.; Boland, J. L.; Snaith, H. J.; Johnston, M. B.; Herz, L. M. Charge-Carrier Dynamics and Mobilities in Formamidinium Lead Mixed-Halide Perovskites. *Adv. Mater.* **2015**, *27* (48), 7938–7944.
- (34) Ruth, A.; Brennan, M. C.; Draguta, S.; Morozov, Y. V.; Zhukovskiy, M.; Janko, B.; Zapol, P.; Kuno, M. Vacancy-Mediated Anion Photo-segregation Kinetics in Mixed Halide Hybrid Perovskites: Coupled Kinetic Monte Carlo and Optical Measurements. *ACS Energy Lett.* **2018**, *3* (10), 2321–2328.
- (35) Zhao, Y.; Miao, P.; Elia, J.; Hu, H.; Wang, X.; Heumueller, T.; Hou, Y.; Matt, G. J.; Osvet, A.; Chen, Y.-T.; et al. Strain-Activated Light-Induced Halide Segregation in Mixed-Halide Perovskite Solids. *Nat. Commun.* **2020**, *11* (1), 1–9.
- (36) Knight, A. J.; Wright, A. D.; Patel, J. B.; McMeekin, D. P.; Snaith, H. J.; Johnston, M. B.; Herz, L. M. Electronic Traps and Phase Segregation in Lead Mixed-Halide Perovskite. *ACS Energy Lett.* **2019**, *4* (1), 75–84.
- (37) Braly, I. L.; Stoddard, R. J.; Rajagopal, A.; Uhl, A. R.; Katahara, J. K.; Jen, A. K.-Y.; Hillhouse, H. W. Current-Induced Phase Segregation in Mixed Halide Hybrid Perovskites and Its Impact on Two-Terminal Tandem Solar Cell Design. *ACS Energy Lett.* **2017**, *2* (8), 1841–1847.
- (38) Chen, S.; Wen, X.; Sheng, R.; Huang, S.; Deng, X.; Green, M. A.; Ho-Baillie, A. Mobile Ion Induced Slow Carrier Dynamics in Organic–Inorganic Perovskite CH₃NH₃PbBr₃. *ACS Appl. Mater. & Interfaces* **2016**, *8* (8), 5351–5357.
- (39) Zhao, Y. C.; Zhou, W. K.; Zhou, X.; Liu, K. H.; Yu, D. P.; Zhao, Q. Quantification of Light-Enhanced Ionic Transport in Lead Iodide Perovskite Thin Films and Its Solar Cell Applications. *Light: Sci. Appl.* **2017**, *6* (5), e16243–e16243.
- (40) Senocrate, A.; Kotomin, E.; Maier, J. On the Way to Optoionics. *Helv. Chim. Acta* **2020**, *103* (7), No. e2000073.
- (41) Bischak, C. G.; Hetherington, C. L.; Wu, H.; Aloni, S.; Ogletree, D. F.; Limmer, D. T.; Ginsberg, N. S. Origin of Reversible Photoinduced Phase Separation in Hybrid Perovskites. *Nano Lett.* **2017**, *17* (2), 1028–1033.
- (42) Bischak, C. G.; Wong, A. B.; Lin, E.; Limmer, D. T.; Yang, P.; Ginsberg, N. S. Tunable Polaron Distortions Control the Extent of Halide Demixing in Lead Halide Perovskites. *J. Phys. Chem. Lett.* **2018**, *9* (14), 3998–4005.